Available online at www.sciencedirect.com
SCIENCE DIRECT
Journal of Catalysis 230 (2005) 359–374
JOURNAL OF CATALYSIS
www.elsevier.com/locate/jcat

Experiments and kinetic model regarding the induction period observed during the oxidation by O_2 of adsorbed CO species on Pt/Al_2O_3 catalysts

Salim Derrouiche, Daniel Bianchi *

Laboratoire d'Application de la Chimie à l'Environnement (LACE), UMR 5634, Université Claude Bernard, Lyon-I, Bat. Raulin, 43 Bd du 11 Novembre 1918, 69622 Villeurbanne, France

Received 11 May 2004; revised 7 December 2004; accepted 15 December 2004

Available online 25 January 2005

Abstract

The present study concerns the characterization, by experiments in the transient regime, at atmospheric pressure, with either a Fourier transform infrared or a mass spectrometer as a detector, of the elementary steps involved in the isothermal oxidation at T_O lower than 360 K of the superficial species formed by adsorption of CO on reduced Pt/Al_2O_3 catalysts: linear, bridged, and threefold coordinated CO species. The coverages of the adsorbed species and the rate of the CO_2 production are determined during successive adsorption, desorption, and oxidation reactions for different durations. The evolution of the rate of the CO_2 production with the duration of the oxidation, RCO2(t), presents a variety of profiles, depending on the Pt dispersion of the catalysts. For Pt dispersions higher than 0.6, an induction period is observed and the RCO2(t) profile is characterized by a peak with a maximum defined by t_m and $RCO2_m$. The greater the Pt dispersion is, the longer t_m is and the lower $RCO2_m$ is. For Pt dispersions lower than 0.6, the RCO2(t) profile is similar to a decreasing exponential, and its highest value is observed at time 0 of the oxidation. The induction period observed for Pt dispersions higher than 0.6 allows us to characterize the Langmuir–Hinshelwood steps between the adsorbed CO and oxygen species by studying the impacts on t_m and $RCO2_m$ of different experimental parameters such as the Pt dispersion, the oxidation temperature, the oxygen partial pressure, and the duration of a desorption stage before oxidation. A kinetic model based on the oxidation of the L CO species by a weakly adsorbed oxygen species formed on the Pt^0 sites liberated by the removal of the bridged CO species provides a set of mathematical expressions that provide a reasonable explanation of the impacts of the various experimental parameters on t_m and $RCO2_m$. As a consequence, this kinetic model reveals how the Pt dispersion affects the elementary step and the turnover frequency of the CO/O_2 reaction. A comparison of the present study with similar literature data on a single Pt crystal shows that the differences in the experimental conditions, material and pressure gaps, may lead to a situation in which the Langmuir–Hinshelwood steps that are studied are not the same.

Keywords: CO/O_2 reaction; Adsorbed CO species; Isothermal; Oxidation; Pt/Al_2O_3; Kinetic model; Microkinetics

1. Introduction

The aim of the microkinetic approach [1] to a gas/solid catalytic reaction is to correlate the kinetic parameters of the surface elementary steps (adsorption, desorption, Langmuir–Hinshelwood steps) involved in a plausible mechanism of the reaction with the turnover frequency (TOF). Different methods can be used to characterize the elementary steps, such as DFT calculations and experimental procedures, either on well-defined single crystal surfaces or on conventional metal-supported catalysts. In previous studies [2–6], this last approach has been developed for the CO/O_2 reaction on Pt/Al_2O_3 catalysts, taking particular account of the presence of different adsorbed CO species on the surface (i.e., linear, bridged, and threefold coordinated CO species, denoted L, B, and 3FC, respectively) [7,8]. It has been shown that the evolution of the TOF during lighting-off tests can be reasonably interpreted by considering that the L CO species (which is the main adsorbed CO species on Pt/Al_2O_3) is the intermediate of the reaction [4,6]. In addition to the

* Corresponding author.
E-mail address: daniel.bianchi@univ-lyon1.fr (D. Bianchi).

0021-9517/$ – see front matter
doi:10.1016/j.jcat.2004.12.011

academic interest of the microkinetic approach, there is a practical perspective: it is conceivable that a correlation can be made between the modifications of the kinetic parameters of each elementary step, and therefore of the TOF, and the catalyst preparation (i.e., dispersion, support), as imagined by Boudart in the foreword of [1]. From this point of view, we have studied the impact of Pt dispersion on the elementary steps involved in the CO/O_2 reaction on Pt/Al_2O_3 [9,10]. Zafaris and Gorte [11] have observed that the TOF of the CO/O_2 reaction is dependent on the size (14 and 1.7 nm) of the Pt particles deposited on a α-$Al_2O_3(0001)$ crystal: the larger the diameter is, the higher the TOF is. We have observed that this is also true on Pt/Al_2O_3 catalysts of different Pt dispersions (range 0.88–0.4) [10]. This is related to the modification of particular elementary steps involved in the kinetic models developed to interpret the TOF [4,6,10]. For instance, it has been shown [10] that the increase in D: (a) decreases the rate constant of oxidation of the adsorbed CO species at low temperatures (particularly the L CO species) and (b) increases the heat of adsorption of the B CO species (denoted EB_{θ_B} at a coverage θ_B). In contrast, the heat of adsorption of the L CO species (denoted EL_{θ_L}) and the reduction of strongly adsorbed oxygen species (denoted O_{sads}) by CO [8] do not depend strongly on D [10].

At high Pt dispersions ($D \gtrsim 0.6$), during the isothermal oxidation by O_2 of the adsorbed CO species, the evolution of the rate of CO_2 production with time on stream t [RCO2(t)] is characterized by an induction period (denoted IP) [10]. It is observed that $RCO_2(t)$ increases slowly for several seconds before a sharp increase followed by a progressive decrease, leading to the detection of a peak characterized by t_m and $RCO2_m$. For $D \lesssim 0.6$ there is no IP; a decreasing exponential profile is observed for RCO2(t) [3,10]. Moreover, the amount of CO_2 formed during the isothermal oxidation indicates clearly that the peak of RCO2(t) is related to the oxidation of the L CO species [10]. Several authors [12–14] have observed the presence of an IP during the isothermal oxidation of adsorbed CO species on noble metal catalysts. They have shown that the duration of IP (measured by t_m) is dependent on: (a) the oxidation temperature T_O and (b) the duration of the desorption t_d in an inert gas before the oxidation. The microkinetic approach to the CO/O_2 reaction developed previously [2–8] has shown that the TOF is correlated at low temperatures with the rate of oxidation of the L CO species according to an L-H step (denoted S3: $L + O_{wads}$ [2,3]) involving a weakly adsorbed oxygen species (denoted O_{wads}) formed only in the presence of adsorbed CO species on the Pt surface (there is no O_{wads} species during the adsorption of O_2 on a freshly reduced Pt/Al_2O_3 catalyst; only O_{sads} species are formed [4]). This leads to the conclusion that the study of the experimental parameters (such as D and P_{O_2}) that control IP, during the isothermal oxidation of the adsorbed CO species, appears to be a way to obtain more insight into the parameters that control this L-H elementary step S3 and therefore the TOF of the CO/O_2 reaction.

The goals of the present article are (a) to study how IP is dependent on several experimental parameters (in line with [12–14]) and (b) to interpret the observations with a kinetic model. To our knowledge this kinetic model has not been used previously for metal-supported catalysts. However, Bonzel and Ku [15] have performed a similar study (experiments and kinetic model) on Pt(110), and a comparison of the respective conclusions is presented to reveal the impact of the material and pressure gaps on the observations linked to the isothermal oxidation of adsorbed CO species.

2. Experimental

2.1. Catalysts

The catalysts used in the present study, y wt% Pt/Al_2O_3, where $y = 1.2$ or 2.9, were the same as those used in previous studies [9,10] [γ-Al_2O_3 (Degussa), BET area 100 m^2/g; incipient wetness method with aqueous solutions of $H_2PtCl_6 \cdot H_2O$ (Aldrich); drying procedure: 12 h at room temperature and then for 24 h at 373 K; pretreatment: 12 h in air at 713 K]. Considering the aims of the present study, we modified the sample reduction procedures [10] as compared with our previous works [2–8] to decrease D progressively. A fresh reduced solid with the highest dispersion ($D > 0.84$) was obtained according to the following procedure (P1), which was also used by Li et al. [14]: He (300 K) → He (423 K, 10 K/min) → H_2 (423 K) → H_2 (713 K, 10 K/min) → H_2 (713 K, 30 min) → He (713 K, 5 min) → He (300 K). The same sample of catalyst was used for several experiments, and it was reduced before each experiment according to the following procedure (P2): He (300 K) → He (723 K, 10 K/min) → H_2 (713 K, 10 min) → He (713 K, 10 min) → O_2 (713 K, 10 min) → He (713 K, 10 min) → H_2 (713 K, 30 min) → He (713 K, 5 min) → He (300 K). It has been observed that D decreased slightly after two successive P2 procedures (from 0.88 to 0.73 after ten P2 procedures with 1.2% Pt/Al_2O_3). The stabilized solids were obtained as follows (P3 procedure): after the P2 procedure, CO was adsorbed at 300 K with the switch He → 2% CO/2% Ar/He, followed by an increase in the temperature (10 K/min) to 713 K. Then after a short helium purge, procedure P2 was applied at 713 K. The stabilization pretreatment with CO, which was initially imposed by the procedure for determination of the heat of adsorption [7,8], led to $D \lesssim 0.65$ for 1.2 and 2.9% Pt/Al_2O_3. Then the subsequent pretreatments, tailored for P2 or P3, decreased D very slowly (lower D value = 0.4).

2.2. Analytical procedures for the study of the elementary steps

The two analytical systems used in the present study were the same as those described in detail in previous studies [2–10]. Mainly, they allowed us to perform experiments in

the transient regime, in which we studied either the molar fractions of the gas with a mass spectrometer or the adsorbed CO species with a FTIR spectrometer. In the first analytical system, various valves allowed us to perform switches between regulated gas flows (1 atm total pressure, flow rate in the range 100–600 cm^3/min), which passed through the catalyst, which was contained in a quartz microreactor. A quadrupole mass spectrometer permitted the determination of the composition (molar fractions) of the gas mixture at the outlet of the reactor during a switch, after a calibration procedure. The temperature was recorded with a small K-type thermocouple ($\Phi = 0.25$ mm) inserted in the catalyst sample (weight ≈ 0.2 g). This system was used to determine the rate of CO_2 production during the isothermal oxidation of the adsorbed CO species at $T_O < 360$ K, with the use of the following switches (100 cm^3/min): He (reduced solid) $\rightarrow$ 1% CO/2% Ar/He (CO adsorption, duration t_a) $\rightarrow$ He (desorption, duration t_d) $\rightarrow$ x% O_2/y% Ar/He (isothermal oxidation, duration t_O) (x, $y < 4$). The duration of the desorption (t_d) varied from 0 to 20 min, whereas that of oxidation (t_O) was a function of the IP. During the oxidation stage, strongly adsorbed oxygen species, O_{sads}, were formed in parallel to the removal of the L CO species by oxidation [3]. The O_{sads} species were reduced to CO_2 with the use of the following switches: x% O_2/y% Ar/He $\rightarrow$ He (purge) $\rightarrow$ 1% CO/2% Ar/He (reduction of the O_{sads} species, duration t_r). The reduction stage is associated with the adsorption of CO [5]; successive isothermal oxidation/reduction of the adsorbed species is denoted as O/R cycles [5]. Because of the strong impact of D on the observations, D is measured by CO or O_2 chemisorption [10] after each reduction procedure (P1, P2, or P3) with the use of the following switches: 1% CO (or O_2)/2% Ar/He (duration t_a, total CO (or O_2) uptake) $\rightarrow$ He (t_d) $\rightarrow$ 1% CO (or O_2)/2% Ar/He (amount of reversible chemisorption). The second analytical system, with a FTIR spectrometer as a detector [2,7,9], allowed us to perform similar experiments in which we studied the evolution of the IR bands of the adsorbed CO species. The solids were compressed to form a disk ($\Phi = 1.8$ cm, $m = 40$–100 mg), which was placed in the sample holder of a stainless-steel IR cell with a small internal volume (transmission mode). This IR cell enabled us to carry out *in situ* treatments (293–900 K) of the solid, at atmospheric pressure, with a gas flow rate in the range of 150–2000 cm^3/min. It must be noted that D was not measured during the FTIR study [10]. To correlate the FTIR observations with the change in D, it was assumed that the decrease in D (quantified with the quartz reactor), according to the number and the nature (P1, P2, P3) of the reduction procedures, was also valid for the catalyst pellet.

2.3. Measurement of the rate of CO_2 production during isothermal oxidation

The main part of the experimental data of the present study concerns the evolution of the rate of CO_2 production during isothermal oxidation of the adsorbed CO species, RCO2(t), with the use of a quartz microreactor. A mass spectrometer provides the molar fraction, $X_g(t)$, of each gas g at the outlet of the reactor, as a function of time on stream in O_2. The rate of CO_2 production is obtained by $\mathrm{RCO2}(t) = X_{CO_2}(t)\ (F/W)$ (in mol/(g s)), where F is the total molar flow rate and W is the weight of catalyst (the figures in the present paper describe the evolution of $X_g(t)$). To determine whether the RCO2(t) corresponds to the RCO2(t) corresponds to the chemical reaction at the surface of the catalyst, the measurements must be free of the contributions of various physical processes (i.e., lag and diffusion processes). Several criteria in the literature make it possible to design experiments that eliminate these physical processes. For instance, we designed the present experiments (as well as those in previous studies) according to the six criteria of Demmin and Gorte (Cr_i) [16], allowing us to evaluate the contribution of several processes to the desorption rate during temperature-programmed desorption in a flow of inert gas. Two of these criteria evaluate the contribution of readsorption during TPD, whereas the other criteria concern the possible contribution of lag and diffusion processes. In a previous study [17] we provided all of the experimental parameters (i.e., reactor geometry, particle sizes) needed to calculate those criteria for the 2.9% Pt/Al_2O_3 catalyst (see Table 1 in [17]). For the present weight of catalyst, $W = 0.2$ g, all of the criteria were either lower or very close to the limits suggested by the authors [16], for instance for a bed concentration gradient the value is 0.18 (suggested < 0.1) and for a particle concentration gradient the value is 0.07 (suggested < 0.05). This supports the assumption that the experimental rate of CO_2 production corresponds to that of the chemical process at the surface of the catalyst. Moreover, according to the method of Rieck and Bell [18], the number of CSTR in series needed to model the bed of catalyst can be determined [17]. For the present experimental conditions this number is 1.1 at 300 K (1.8 in [17] for $W = 0.3$ g), and this value decreases slightly with the increase in T. Other criteria can be used to design experiments free of physical processes [19]. For instance, if we consider Table 1 in [17], the absence of internal diffusion can be justified by evaluation of the Thiele modulus, Φ [19], with the use of an effective diffusion coefficient of 3×10^{-3} cm^2/s and assuming an oxygen conversion of 50% at the maximum of the CO_2 peak for a 1% O_2/1% Ar/He mixture (the experimental O_2 conversions are lower); then $\Phi = 0.867$, leading to an effectiveness factor $\eta > 0.95$ [19]. The above criteria make it possible to design experiments free of the contributions of various physical processes to the rate of the CO_2 production under pseudo-stationary conditions. However, during the initial stage of the transient (i.e., at the introduction of O_2), the diffusion processes cannot be prevented because the rate of adsorption of a gas is too high (i.e., the effectiveness factor is very low). In the present study the $X_{CO_2}(t)$ values during the first seconds ($\lesssim 20$ s) of the transient are not considered.

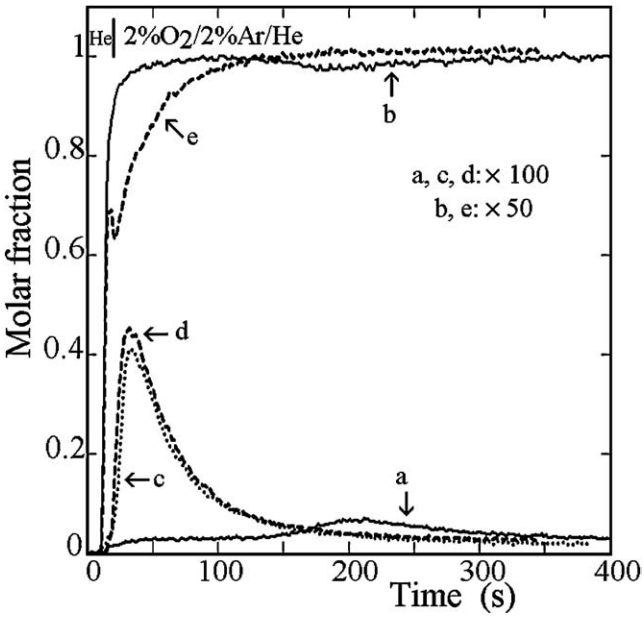

Fig. 1. Molar fractions of the gas at the outlet of the micro reactor during the oxidation at 300 K using 2% O_2/2% Ar/He of the adsorbed CO species on a fresh ($D = 0.73$) and stabilized ($D = 0.54$ and $D = 0.48$) 2.9% Pt/Al_2O_3 ($t_d = 80$ s): (a) CO_2 and (b) O_2 for $D = 0.73$; (c) CO_2 for $D = 0.54$; (d) CO_2 and (e) O_2 for $D = 0.48$.

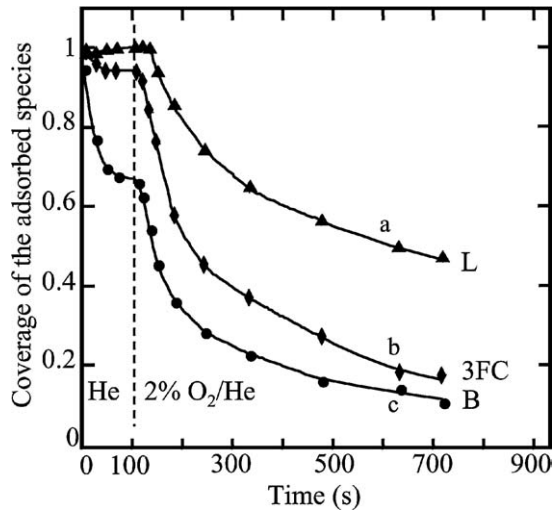

Fig. 2. Evolution of the coverages of the adsorbed CO species at 300 K on 1.2% Pt/Al_2O_3 with $D \approx 0.7$ during desorption in helium and oxidation with 2% O_2/He. (a) L CO species, (b) 3FC CO species, and (c) B CO species.

3. Results and discussion

On highly dispersed Pt/Al_2O_3 catalysts ($D \gtrsim 0.6$), it has been shown [10], in agreement with data in the literature [12–14], that the rate of CO_2 production, RCO2(t), during isothermal ($T_O < 353$ K) oxidation by O_2 of the adsorbed CO species is characterized by an IP leading to the observation of a peak (characterized by t_m and $RCO2_m$) after several seconds of oxidation. The duration of the IP is conventionally measured by t_m [10,12–14]. Moreover, the adsorption of CO on Pt/Al_2O_3 leads mainly to the formation of the L CO species ($\approx$92% of the amount of adsorbed CO for $D < 0.5$ [10]), and RCO2(t) is dominated by the oxidation of this adsorbed species, particularly during the detection of the RCO2(t) peak [10]. The intent of the present study is to describe the impacts of different experimental parameters on IP and to interpret observations made with a kinetic model. The focus of this study is the assumption that the L CO species is involved in the L-H elementary step that controls the TOF during the CO/O_2 reaction at low temperatures.

3.1. Impacts of the experimental parameters on the oxidation of the adsorbed CO species

3.1.1. Impact of D

This parameter has been studied in more detail in [10]; we summarize the main observations to facilitate the presentation. Fig. 1 compares the molar fractions of CO_2 and O_2 at the outlet of the reactor during the oxidation at 300 K on 2.9% Pt/Al_2O_3 for three D values ($D = 0.73$, 0.54, 0.48) with the following switches: pretreatment $\rightarrow$ 1% CO/2% Ar/He (adsorption of L, B, and 3FC species) $\rightarrow$ He ($t_d = 80$ s) $\rightarrow$ 2% O_2/2% Ar/He (t_o). Fig. 1 shows that at the highest dispersion, RCO2(t) is characterized by an IP; clearly, the higher D is, the longer t_m is and the lower $RCO2_m$ is. At the lowest dispersion the CO_2 peak is observed at the introduction of O_2, as studied previously [2,3]. This impact of D on the IP has not been considered previously [12–14]. In Fig. 1, the amount of CO_2 produced during the RCO2(t) peak is compatible only with the oxidation of the L CO species.

Fig. 2 compares the evolution of the coverage of the adsorbed CO species (derived from their specific IR bands [8,10]) at 300 K on 1.2% Pt/Al_2O_3 after the following pretreatment: two successive P2 procedures (estimated D value $\approx$ 0.7–0.75), with the switches 1% CO/He $\rightarrow$ He (t_d) $\rightarrow$ 2% O_2/He (t_O) (see more details in [10]). It can be observed in Fig. 2a that the isothermal desorption in helium has no impact on the IR band of the L CO species (high heat of adsorption of the L CO species [7–9]), whereas those of the 3FC and B CO species decrease to pseudo-stationary values after $\approx$2 min (Figs. 2b and c). The introduction of O_2 (Fig. 2) strongly increases the rate of disappearance of the B and 3FC CO species, whereas the decrease in the L CO species during the oxidation is delayed by $\approx$40 s. The results in Fig. 2 show that the first part of the IP in Fig. 1 must be correlated with the removal of the B or/and 3FC CO species, whereas the $RCO_2(t)$ peak is mainly due to the L CO species.

3.1.2. Impact of the oxidation temperature

Fig. 3 shows the impact of T_O on the IP for the 2.9% Pt/Al_2O_3 catalyst at $D = 0.73$, with 2% O_2/2% Ar/He after $t_d = 80$ s and for the first O/R cycle. It can be observed that the higher T_O is, the shorter t_m is. This has been observed by several authors [12–14] on Pt and Pd catalysts. Zhou and Gulari [13], from their study of Pd/Al_2O_3, have de-

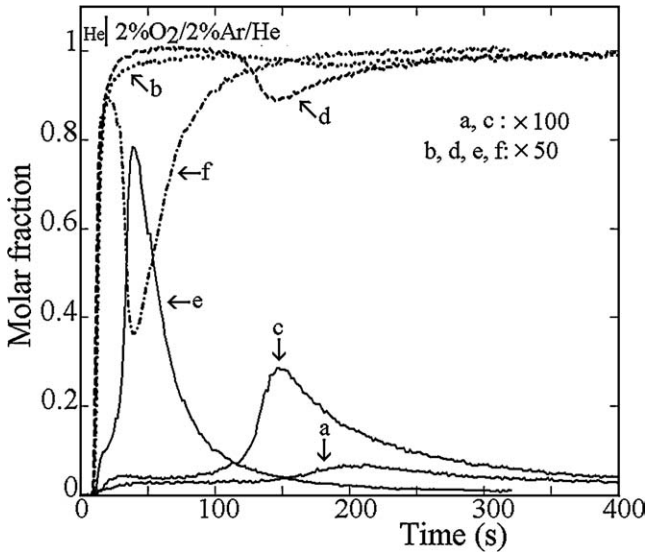

Fig. 3. Molar fractions of the gas at the outlet of the micro reactor during the oxidation at three temperatures using 2% O_2/2% Ar/He of the adsorbed CO species on 2.9% Pt/Al_2O_3 with $D = 0.73$ ($t_d = 80$ s): (a) CO_2 and (b) O_2 for $T_O = 298$ K; (c) CO_2 and (d) O_2 for $T_O = 324$ K; (e) CO_2 and (f) O_2 for $T_O = 351$ K.

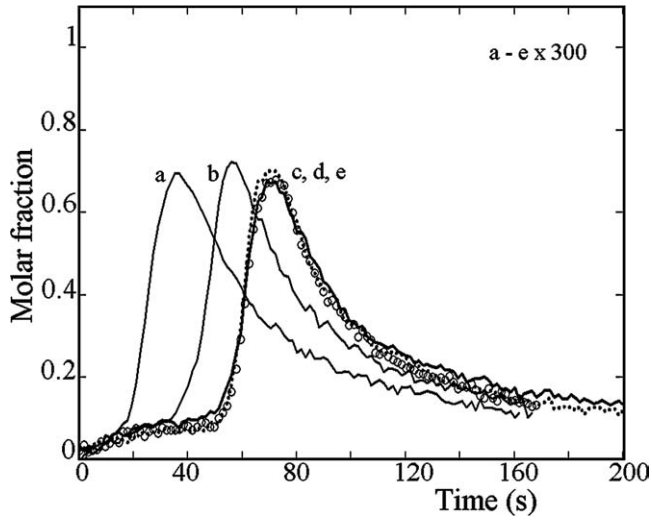

Fig. 4. Molar fractions of CO_2 at the outlet of the micro reactor during the oxidation at $T_O = 324$ K using 2% O_2/2% Ar/He of the adsorbed CO species on a 1.2% Pt/Al_2O_3 with $D = 0.63$ ($t_d = 80$ s) as a function of the number of successive O/R cycles: (a)–(e) cycle numbers 1, 2, 3 4, and 8, respectively.

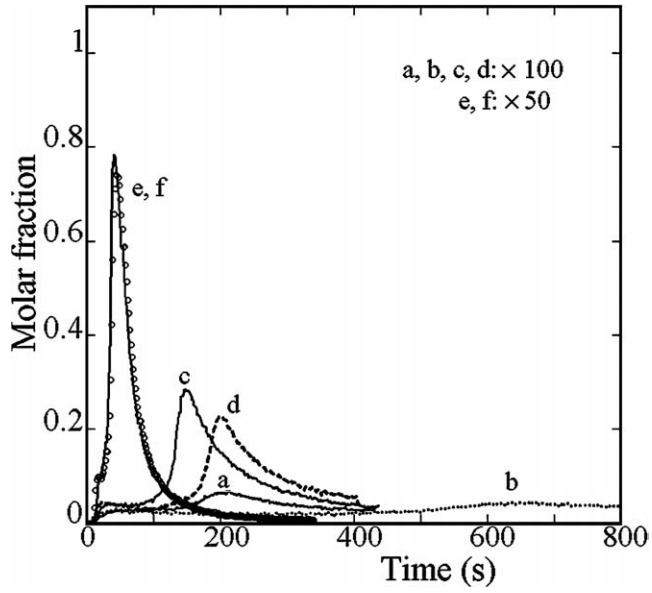

Fig. 5. Molar fractions of CO_2 at the outlet of the micro reactor during the oxidation at three temperatures using 2% O_2/2% Ar/He of the adsorbed CO species on 2.9 % Pt/Al_2O_3 with $D = 0.74$ ($t_d = 80$ s) for the two first O/R cycles: (a) and (b) first and second cycle for $T_O = 298$ K; (c) and (d) first and second cycle for $T_O = 323$ K; (e) and (f) first and second cycle for $T_O = 353$ K.

cided that this proves that the IP is not linked to mass transfer processes (in agreement with the design of the present experiments). Moreover, they have shown that $\ln(t_m) = f(1/T_O)$ is a straight line and the positive slope is used (without a kinetic model) to determine an apparent activation energy of 90 kJ/mol for the chemical process associated with the IP [13]. It can be observed in Fig. 3 that there is an oxygen consumption associated with CO_2 production and that CO_2 is not due to desorption (i.e., carbonates). Moreover, the rate of the oxygen consumption is twice that of the CO_2 production, indicating that the removal of the L CO species is associated with the adsorption of strongly adsorbed oxygen species, O_{sads}, which is in line with previous works [2,3].

3.1.3. Impact of the number of isothermal O/R cycles

Fig. 4 shows the evolution of RCO2(t) at $T_O = 324$ K on 1.2% Pt/Al_2O_3 ($D = 0.63$) with the number of O/R cycles. After oxidation of the adsorbed CO species, the following switches were performed: 2% O_2/2% Ar/He (oxidation) → He (80 s) → 1% CO/2% Ar/He (reduction of O_{sads} by CO) → He ($t_d = 80$ s) → 2% O_2/2% Ar/He (oxidation). This constitutes an O/R cycle, and the experiments can be repeated (without any pretreatment at 713 K) for the study of the impact of several O/R cycles on the IP. It can be observed in Fig. 4 that t_m increases for three successive O/R cycles, and then the observations are reproducible. Fig. 5 shows similar observations for 2.9% Pt/Al_2O_3 ($D = 0.73$) comparing the first and second O/R cycles at three T_O values. For $T_O \leqslant 324$ K, it is clear that the first O/R cycle increases t_m as in Fig. 4, whereas at 353 K, the number of O/R cycles has no impact. The increase in t_m with the number of O/R cycles indicates that the reactivity of the Pt surface changes because of irreversible modifications of the adsorbed species/Pt surface system. For instance, it has been shown [5] that (a) strongly adsorbed oxygen species, O_{sads}, are formed on the Pt sites liberated by the removal of the L CO species during their oxidation (see Fig. 3) and (b) a fraction of these O_{sads} species remain on the surface after the reduction stage (the activation energy of reduction increases with the decrease in the coverage of the O_{sads} species [5]) and may modify the reactivity of the surface. Moreover, it has been observed that during the first O/R cycle a small

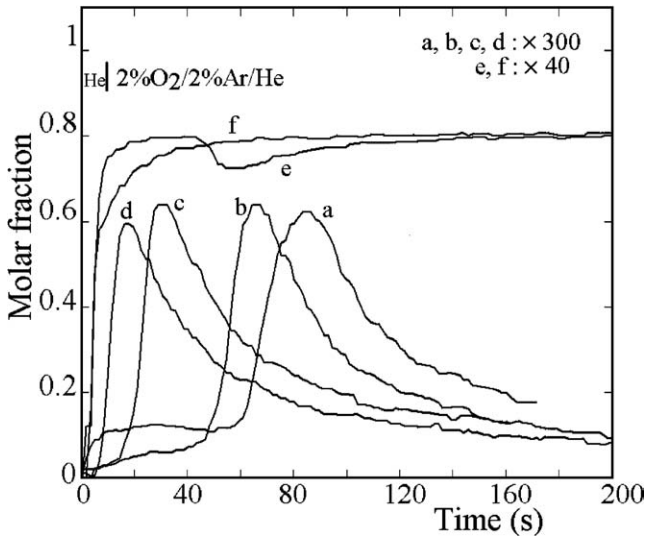

Fig. 6. Molar fractions of the gas at the outlet of the micro reactor during the oxidation at 324 K using 2% O_2/2% Ar/He of the adsorbed CO species on 1.2% Pt/Al_2O_3 with $D = 0.63$ after three O/R as a function of the desorption duration t_d: (a) to (d) CO_2 for $t_d = 0$ s, 80 s, 6 min and 15 min respectively; (e) and (f) O_2 for $t_d = 80$ s and 15 min, respectively.

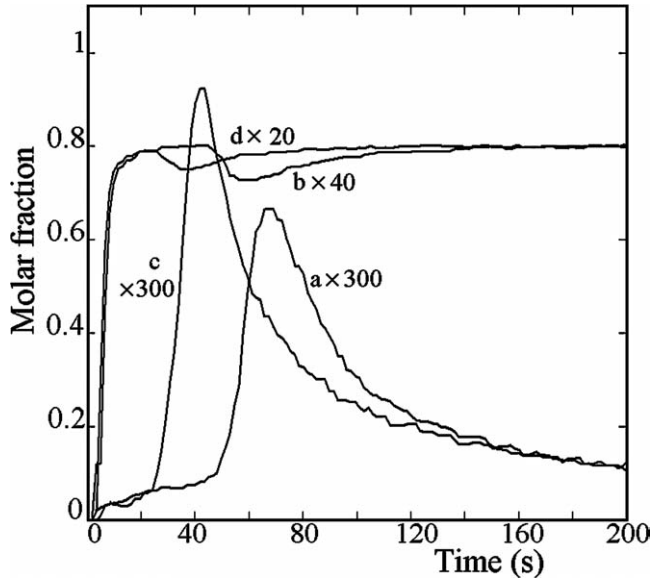

Fig. 7. Molar fractions of the gas at the outlet of the micro reactor during the oxidation at 323 K of the adsorbed CO species on 1.2% Pt/Al_2O_3 with $D = 0.63$ ($t_d = 80$ s) as a function of the oxygen partial pressure: (a) CO and (b) O_2 for $PO_2 = 2$ kPa; (c) CO_2 and (d) O_2 for $P_{O_2} = 4$ kPa.

number of Pt^0 sites are irreversibly transformed into Pt^{2+} [2,10] (only a reduction stage at high temperatures eliminates the Pt^{2+} sites). However, Fig. 4 shows that the RCO2(t) profile is reproducible after three O/R cycles at $T_O = 324$ K, indicating that the surface modifications are over. It must be noted in Fig. 4 that if the number of O/R cycles affects t_m, it does not have a strong impact on $RCO2_m$. Fig. 5 shows that the impact of the number of O/R cycles disappears for $T_O = 353$ K; this means that the O_{sads} species involved in the surface modifications are removed by the reduction stage. The study of the following experimental parameters is performed after at least two O/R cycles.

3.1.4. Impact of the duration of the isothermal desorption (t_d) before the oxidation

The impact of t_d on t_m (after three O/R cycles) is shown in Fig. 6 for 1.2% Pt/Al_2O_3 ($D = 0.63$). The situation $t_d = 0$ corresponds to the switch 1% CO/2% Ar/He → 2% O_2/2% Ar/He without any helium purge. It can be observed that the longer t_d is, the shorter t_m is. This has been observed previously by several authors [12–14], and the qualitative explanation for this is that either some particular Pt sites are created because of the desorption of an adsorbed CO species [12,14] or there is a restructuring/reconstruction of the CO_{ads}/Pt system to a more favorable state (without any significant CO desorption) [13]. Moreover, Fig. 6 shows that if t_d affects t_m significantly, it does not have a strong impact on $RCO2_m$.

3.1.5. Impact of the oxygen partial pressure

Fig. 7 compares the RCO2(t) profiles at 323 K on 1.2% Pt/Al_2O_3 ($D = 0.63$) for two O_2 partial pressures: $P_{O_2} =$ 2 kPa and 4 kPa (after three O/R cycles). It can be observed that the higher P_{O_2} is, the shorter t_m is and the higher $RCO2_m$ is. We have shown previously that in the absence of an IP ($D < 0.5$), the rate of oxidation of the L CO depends on $P_{O_2}^{1/2}$ [2,3]. The results in Fig. 7 show that for $D > 0.6$ and in the presence of an IP, RCO2(t) also depends on P_{O_2} (the exact relationship between RCO2(t) and P_{O_2} is provided by the kinetic model).

3.2. Qualitative interpretation of the induction period

Regardless of the value of D, the adsorption of CO leads mainly to the formation of the L CO species [9,10], and the amounts of CO_2 produced during the RCO2(t) peaks in Figs. 1, 3–7 are compatible only with the oxidation of this adsorbed species. The L-H elementary step (denoted S3: L CO + O_{wads} → CO_{2ads} [2–4]) linked to the oxidation of the L CO species has been studied previously for $D < 0.5$ [2–4], and it has been shown that a weakly adsorbed oxygen species formed without competition with the L CO species O_{wads} is involved [2–4] in the reaction. The rate of CO_2 formation by the oxidation of the L CO species is given by [2–4]

$$\mathrm{RCO2L}(t) = \frac{-\mathrm{d}\theta_L}{\mathrm{d}t} = k_3\theta_L\theta_{O_{wads}}, \quad (1)$$

where θ_L and $\theta_{O_{wads}}$ are, respectively, the coverages of the L and O_{wads} species on different Pt sites and k_3 is the rate constant of step S3 [2–4]. It has been shown that the heat of adsorption of the L CO species, EL_{θ_L}, is not significantly modified by D [9]. The EL_1 value 110 kJ/mol indicates that the L CO species cannot desorb at $T < 353$ K, in agreement with Fig. 2. This leads to the conclusion that it is not a modification of θ_L by the increase in D that explains the IP. The impact of D on RCO2(t) must concern k_3 and/or $\theta_{O_{wads}}$. For

$D < 0.5$ it has been shown [2] that k_3 remains constant for a large variation of θ_L. This leads us to consider the possibility, as suggested by several authors [12–14], that the IP is due to the increase in the number of Pt^0 sites adsorbing the oxygen species (these sites are denoted s1 in the present paper). In the literature [12–14], this increase is mainly ascribed to the desorption of an adsorbed CO species. We have suggested [4,6] that the s1 sites are formed by the removal of the B CO species (on particular Pt sites denoted Pt^0_B) because the EB_{θ_B} values (lower than EL_{θ_L} [8,10]) are compatible with a desorption at 300 K. However, Fig. 2 shows that the 3FC CO species also desorbs slightly at low temperatures, and it can also be involved in the formation of the $s1$ sites. Nevertheless, in the present paper, to simplify the presentation of the kinetic model, we assign the IP process to the removal of the B CO species. The number of $s1$ sites for the adsorption of O_{wads} is dependent on (a) the total amount of Pt^0_B sites adsorbing the B CO species (denoted NT_B, $< 8\%$ of the total number of Pt sites) and (b) the amount of those sites free of B CO species at time t of the oxidation. At time $t = 0$ of the oxidation, the number of $s1$ sites is determined by the desorption of the B CO species during the helium purge according to (a) the activation energy of desorption of the B CO species (which increases with the decrease in θ_B [9] and with the increase in D [10]) and (b) the duration t_d of the desorption stage. For instance, it is expected that for a fixed t_d, the number of $s1$ sites at time 0 of the oxidation is higher for a low than for a high dispersion because of a decrease in the activation energy of desorption of the B CO species with the decrease in D. During the oxidation and according to the views of [12–14], it can be assumed that the desorption of the B CO species continues to create the $s1$ sites. However, Fig. 2 shows clearly that the rate of disappearance of the B CO species increases with the introduction of O_2. This indicates that either there is a competitive chemisorption between the oxygen and the B CO species or that an oxidation of the B CO species contributes to their removal. The absence of a significant molar fraction of CO at the outlet of the reactor at the introduction of O_2 does not support the competitive adsorption, whereas a fraction of the CO_2 production during the initial part of the IP can be associated with the oxidation of the B CO species. This allows us to assume that the IP is mainly linked to the increase in the number of $s1$ sites by oxidation of the B CO species. This oxidation has (a) a limited impact on the amount of CO_2 production (B CO species represent less that 8% of the total amount of adsorbed CO) and (b) a strong impact on the increase in the number of $s1$ sites. In summary, as compared with the literature data that evoke only a desorption process for the formation of the $s1$ sites, we believe that this process is due to (a) the desorption of the B CO species during the helium purge before the oxidation and (b) mainly the oxidation of the B CO species in the presence of O_2. The qualitative explanation of the IP, taking into consideration the increase in the number of $s1$ sites during oxidation, is as follows [12–14]: (a) at high coverage of the Pt surface by the adsorbed CO species, the formation of new $s1$ sites adsorbing O_2 leads to a progressive increase in $RCO2(t)$ during the initial stage of the isothermal oxidation and (b) the exhaustion of the L CO species on the surface decreases $RCO2(t)$, leading to the observation of a peak for $RCO2(t)$ characterized by t_m and $RCO2_m$. This qualitative interpretation of IP is insufficient in the view of the microkinetic approach and inexact for specific experimental conditions. For instance, in a previous work [20] on the isothermal hydrogenation into CH_4 of adsorbed carbonaceous species, it has been shown that the increase in the number of sites adsorbing hydrogen must conform to a particular criterion for the observation of a peak in the rate of the CH_4 production. The kinetic model developed below, to interpret the IP during the isothermal oxidation of the adsorbed CO species, leads to a similar conclusion.

3.3. Kinetic model of the oxidation of adsorbed CO species on Pt/Al_2O_3 at low temperatures

3.3.1. Surface elementary steps

According to the qualitative interpretation, the plausible elementary steps involved in the IP of the isothermal oxidation of the adsorbed CO species are as follows:

Step Sa. Desorption of the B CO species and the formation of $s1$:

$$B_{ads} \rightarrow CO + x\,s1,$$

where the rate constant is k_{dB}; activation energy of desorption E_{dB} equal to the heat of adsorption of the B CO species (nonactivated chemisorption).

Step Sa is the single elementary step during the helium purge before oxidation. The stoichiometric coefficient x is introduced to take into account the fact that we do not know the number of Pt^0 sites adsorbing the B CO species that must be liberated to create one $s1$ site for the formation of O_{wads} ($x \leqslant 1$).

Step S2. The adsorption/desorption equilibrium (because of the large O_2 excess) of O_{wads} on the $s1$ sites (notation used in [2–4]):

$$O_{2(gas)} \Leftrightarrow 2O_{wads},$$

where adsorption coefficient $K_{O_2} = k_{aO_2}/k_{dO_2}$; k_{aO_2} and k_{dO_2} are, respectively, the rate constants of adsorption and desorption of the O_{wads} species, with a heat of adsorption $E_{O_2} = E_{O_2d} - E_{O_2a}$ (E_{O_2a} and E_{O_2d} are, respectively, the activation energies of adsorption and desorption).

Step Sb. The L-H step for the oxidation of the B CO species and the formation of $s1$ sites:

$$B + O_{wads} \rightarrow CO_2 + x\,s1,$$

where the rate constant is k_{O_B} and activation energy is E_{O_B}.

Step S3. The L-H step for the oxidation of the L CO species (this L-H step has been previously studied for $D < 0.5$ [2–4]):

$$L + O_{wads} \rightarrow CO_2 + Pt^0_L,$$

where the rate constant is k_3 and activation energy is E_3.

The amount of CO_2 produced in the peaks in Figs. 1, 3–7 come mainly from step S3 (the L CO species is the main adsorbed species), whereas step Sb contributes to CO_2 production during the induction period. The Pt_L sites in step S3 adsorb O_2 to form strongly adsorbed O_{sads} species in parallel to the removal of the L CO species (Fig. 3 and [2,3]). However, the O_{sads} species do not contribute significantly to the oxidation of the L CO species (see Fig. 7 in [2]) because they have a low reactivity at low coverages [5].

3.3.2. *Mathematical formalism linked to the induction period*

From the elementary steps Sa, S2, Sb, and S3 a set of differential equations can be formulated and then solved numerically to determine the evolutions of the surface concentrations of L, B, $s1$, and of the rate of CO_2 production, with the use of acceptable values of the different kinetic parameters to obtain the best agreement between theoretical and experimental curves. However, a mathematical solution is available that takes into consideration reasonable simplifying assumptions linked to the experimental observations. This provides mathematical expressions that clearly quantify the impact of the main kinetic parameters on IP. The following simplifications are adopted:

(a) The experimental rate of CO_2 production, RCO2(t) (Figs. 1, 3–7), is the sum of the rate of oxidation of the L CO species (denoted RCO2L(t)) from step S3 and of the B CO species (denoted RCO2B(t)) from step Sb. Considering that the L CO species dominates the CO adsorption (>92% of the amount of adsorbed CO), it is assumed that the RCO2(t) peak in Figs. 1, 3–7 is due only to RCO2L(t), whereas RCO2B(t) contributes to RCO2(t) during the initial stage of the IP. This leads us to assume that the kinetic model of the experimental RCO2(t) peaks in Figs. 1, 3–7 is linked to RCO2L(t).

(b) The O_{wads} species are formed on the $s1$ sites liberated by the removal of the B CO species either by step Sa during the helium purge before oxidation or by steps Sa and Sb during the oxidation. However, considering Fig. 2, it is assumed that step Sa is negligible as compared with step Sb during oxidation.

(c) Step S2 is considered at the adsorption equilibrium on the available $s1$ sites. The amount of O_{wads} species (i.e., surface concentration) increases during the oxidation because of the increase in the number of $s1$ sites (step Sb), whereas the coverage of those sites, $\theta_{O_{wads}}$, remains constant. Considering the Langmuir's model for weakly adsorbed dissociative species, the coverage of the O_{wads} species is [2–4]

$$\theta_{O_{wads}} \approx \sqrt{K_{O_2} P_{O_2}}. \tag{2}$$

From assumption (a), the kinetic model of RCO2L(t) must allow one to explain the RCO2(t) peak in Figs. 1, 3–7. From the classical formalism of the rate of a L-H elementary in term of coverages (mean-field approximation), RCO2L(t) is given by expression (1). The pre-exponential factor of the rate constant of an L-H step such as Sb and S3 used in the classical kinetic model is 10^{12} to 10^{14} s^{-1} [21–23], and in the present study it is considered equal to $kT/h \approx 10^{13}$ s^{-1}, where k and h are Boltzmann's and Planck's constants, respectively. The formalism of expression (1) is not adapted to take into account the increase in the number of $s1$ sites according to steps Sa and Sb. It is more informative to use the superficial concentrations of the different sites and adsorbed species: molecules (or sites) per unit surface area (cm^2) of Pt surface. For instance, expression (1) can be modified as follows (with the notation of steps Sa, S2, Sb, and S3):

$$\frac{-\mathrm{dL}(t)}{\mathrm{NT_L}\,\mathrm{d}t} = k_{3(s)} \frac{L(t)}{\mathrm{NT_L}} \theta_{O_{wads}} \Rightarrow \frac{-\mathrm{dL}(t)}{\mathrm{d}t} = k_{3(s)} \mathrm{L}(t) \theta_{O_{wads}}, \tag{3}$$

where (a) NT_L represents the highest surface concentration of L CO species (this species dominates the CO adsorption and roughly $NT_L \approx 10^{14}$ to 10^{15} molecules/cm^2, assuming a Pt atomic radius of 1.39×10^{-10} m [21]); (b) L(t) is the surface concentration of the L CO species after a duration t of the oxidation: at time $t = 0$ (after a desorption duration t_d), $L(0) = NT_L$ because the L CO species is strongly adsorbed; (c) the notation $k_{3(s)}$ indicates that the unit of the rate constant is s^{-1}. The coverage of the O_{wads} species at time t of the oxidation is

$$\theta_{O_{wads}} = \frac{\mathrm{QO_{wads}}(t)}{\mathrm{S1_M}}, \tag{4}$$

where (a) $QO_{wads}(t)$ is the surface concentration of O_{wads} species after an oxidation duration t and (b) $S1_M$ is the highest number of $s1$ sites that can be available for the adsorption of the O_{wads} species. This number is linked by the factor x to NT_B, the total number of Pt sites adsorbing the B CO species ($NT_B \approx 0.08$ ($NT_L + NT_B$) for $D \approx 0.5$ [10]). The ratio between the amount of B and L CO species decreases slightly with the increase in D. For instance, on 2.9% Pt/Al_2O_3 the ratio of the IR band intensities B CO/ L CO increases from 0.124 to 0.132 after the P1 procedure and six P3 + P2 procedures, respectively. This is line with the study of Sarkany and Gonzalez [24], who have observed that the ratio of the IR band intensities of the B CO/ L CO species increases from 0.19 to 0.23 on a 6% Pt/Al_2O_3 catalyst, whereas the Pt dispersion decreases from 0.57 (ratio CO/Pt = 0.7) to 0.12 (ratio CO/Pt = 0.52). The authors conclude that the percentage of B CO species is larger at a lower dispersion [24]. Similarly, Vannice et al. [25] have shown that the ratio CO (L and B CO species)/Pt_s (Pt_s measured by hydrogen chemisorption) increases slightly with a decrease in particle size (see Table 2 in [25]), indicating that the L CO species is favored at high dispersions. The fact that high Pt dispersions decrease the proportion of B CO species is probably linked to the modification of the structure of the particles. For instance, Hayden et al. [26] have shown by IRAS that the adsorption of CO leads to the formation of L and the B CO species on Pt(111), whereas there

is no B CO species on a stepped surface. Finally, it is reasonable to assume that the ratio B CO/L CO decreases with a increase in D, and we assume that roughly NT_B is approximately $\leqslant 0.1\ NT_L$ in sites/cm^2 of Pt surface, regardless of the value of D. The substitution of (4) in (3) leads to

$$\frac{-\mathrm{dL}(t)}{\mathrm{d}t} = k_{3(s)}\mathrm{L}(t)\frac{\mathrm{QO_{wads}}(t)}{\mathrm{S1_M}} = k_3\mathrm{L}(t)\mathrm{QO_{wads}}(t), \quad (5)$$

where the unit of the pre-exponential factor of k_3 on the right side of (5) is cm^2/(sites s), with a value roughly equal to $\approx (kT/h)/(0.1\times 10^{15}) = 10^{-1}$ cm^2/(molecule s^{-1}), which is a value similar to that estimated for Pt(111) at low coverage of the reactants [23]. In (5), $\mathrm{QO_{wads}}(t) = \mathrm{S1}(t)\ \theta_{\mathrm{O_{wads}}}$, where $\mathrm{S1}(t)$ is the number of $s1$ sites effectively free for the activation of O_2, because of the removal of the B CO species. Considering weakly adsorbed oxygen species, expression (2) indicates that $\theta_{\mathrm{O_{wads}}} \ll 1$ and $\mathrm{QO_{wads}} \ll \mathrm{S1}(t)$, regardless of t. Finally, expression (5) gives the rate of the CO_2 production (molecules/(cm^2 s)) from the oxidation of L CO species (step S3)

$$\mathrm{RCO2L}(t) = \frac{-\mathrm{dL}(t)}{\mathrm{d}t} = k_3 L(t)\theta_{\mathrm{O_{wads}}}\mathrm{S1}(t). \quad (6)$$

Similarly, according to step Sb, the rates of disappearance of the B CO species during the oxidation (rate of CO_2 production: $\mathrm{RCO2B}(t)$) and of the appearance of the $s1$ sites are given by

$$\frac{\mathrm{dS1}(t)}{x\,\mathrm{d}t} = \frac{-\mathrm{dB}(t)}{\mathrm{d}t} = \mathrm{RCO2B}(t) = k_{\mathrm{O_B}}\mathrm{B}(t)\theta_{\mathrm{O_{wads}}}\mathrm{S1}(t), \quad (7)$$

where $\mathrm{B}(t)$ is the surface concentration of B CO species at time t of the oxidation. The left side of expression (7) allows one to determine the relationship between $\mathrm{S1}(t)$ and $\mathrm{B}(t)$ during the oxidation:

$$\mathrm{S1}(t) + x\mathrm{B}(t) = \mathrm{S1}(0) + x\mathrm{B}(0) = N_0, \quad (8)$$

where S1(0) and B(0) are the surface concentrations of $s1$ and B CO species at time 0 of the oxidation: their values are fixed by the desorption stage before the oxidation according to t_d and E_{dB}. During this helium purge only step Sa is operative, and it leads to an expression similar to (8) (with t' denoting the time on stream in helium)

$$\mathrm{S1}(t') + x\mathrm{B}(t') = \mathrm{S1}(t'=0) + x\mathrm{B}(t'=0). \quad (9)$$

The $\mathrm{B}(t'=0)$ value is provided by the adsorption equilibrium of the B CO species at 300 K for $P_{CO} = 1$ kPa [10]: ≈ 1 and ≈ 0.85 on highly ($D \gtrsim 0.6$) and on lowly ($D \lesssim 0.6$) dispersed Pt catalysts due to the decrease in EB_1 with the decrease in D [10]. The IP is linked to $D > 0.6$, giving $\mathrm{B}(t'=0) = \mathrm{NT_B}$ and $\mathrm{S1}(t'=0) = 0$ and, finally, after a duration $t' = t_d$ of the desorption,

$$\mathrm{S1}(t_d) = x\big(\mathrm{NT_B} - \mathrm{B}(t_d)\big). \quad (10)$$

Expression (10) provides the relationship between the various sites involved in the activation of $\mathrm{O_{wads}}$ at time $t = 0$ of the oxidation:

$$\mathrm{S1}(0) = x\big(\mathrm{NT_B} - \mathrm{B}(0)\big) \quad \text{or} \quad N_0 = x\mathrm{NT_B}$$
(considering relation (8)). (11)

B(0) is the amount B CO species at the end of the desorption. Expressions (7) and (8) give

$$\frac{\mathrm{dS1}(t)}{\mathrm{S1}(t)(N_0 - \mathrm{S1}(t))} = k_{\mathrm{O_B}}\theta_{\mathrm{O_{wads}}}\,\mathrm{d}t, \quad (12)$$

which after integration (at $t = 0$, S1(0)) provides $\mathrm{S1}(t)$

$$\mathrm{S1}(t) = \left(\frac{N_0\mathrm{S1}(0)}{N_0 - \mathrm{S1}(0)}\right)\left[\frac{1}{\frac{\mathrm{S1}(0)}{N_0 - \mathrm{S1}(0)} + \exp(-k_{\mathrm{O_B}}N_0\theta_{\mathrm{O_{wads}}}t)}\right]. \quad (13a)$$

Considering $\mathrm{S1}(0) = (N_0 - x\mathrm{B}(0))$ from (8) and $N_0 = x\mathrm{NT_B}$ (11), then (13a) gives

$$\mathrm{S1}(t) = \left(\frac{x\mathrm{NT_B}(\mathrm{NT_B} - \mathrm{B}(0))}{\mathrm{B}(0)}\right) \times \left[\frac{\exp(k_{\mathrm{OB}}N_0\theta_{\mathrm{O_{wads}}}t)}{1 + \frac{\mathrm{NT_B} - \mathrm{B}(0)}{\mathrm{B}(0)}\exp(k_{\mathrm{OB}}N_0\theta_{\mathrm{O_{wads}}}t)}\right]. \quad (13b)$$

$\mathrm{RCO2L}(t)$ presents a peak for $\mathrm{d}(\mathrm{RCO2L}(t))/\mathrm{d}t = 0$. Expression (6) shows that this corresponds to

$$\mathrm{S1}(t)\frac{\mathrm{dL}(t)}{\mathrm{d}t} + \mathrm{L}(t)\frac{\mathrm{dS1}(t)}{\mathrm{d}t} = 0. \quad (14)$$

Expression (14) can be modified with the use of expressions (6) and (12), and the amount of S1 sites at the maximum of $\mathrm{RCO2L}(t)$ (after a duration t_m of the oxidation) is given by

$$\mathrm{S1}(t_m) = \frac{k_{\mathrm{O_B}}N_0}{k_{\mathrm{O_B}} + k_3}. \quad (15)$$

Expressions (13a) and (15) provide t_m

$$t_m = \left(\frac{1}{k_{\mathrm{O_B}}N_0\theta_{\mathrm{O_{wads}}}}\right)\ln\left[\left(\frac{N_0}{\mathrm{S1}(0)} - 1\right)\frac{k_{\mathrm{O_B}}}{k_3}\right]. \quad (16)$$

The substitution in (16) of N_0, S1(0), and $\theta_{\mathrm{O_{wads}}}$ from expressions (8), (11), and (2), respectively, leads to

$$t_m = \left(\frac{1}{k_{\mathrm{O_B}}x\mathrm{NT_B}\sqrt{K_{\mathrm{O_2}}P_{\mathrm{O_2}}}}\right)\ln\left[\left(\frac{\mathrm{B}(0)}{\mathrm{NT_B} - \mathrm{B}(0)}\right)\frac{k_{\mathrm{O_B}}}{k_3}\right]. \quad (17)$$

A positive t_m value requires that

$$\left(\frac{\mathrm{B}(0)}{\mathrm{NT_B} - \mathrm{B}(0)}\right)\frac{k_{\mathrm{O_B}}}{k_3} \geqslant 1 \quad \text{or} \quad \mathrm{B}(0) \geqslant \frac{\mathrm{NT_B}k_3}{k_{\mathrm{O_B}} + k_3}. \quad (18)$$

The advantage of expression (17) as compared with a numerical solution of the differential equations is to reveal the main impacts of the experimental and kinetic parameters on the IP: seven parameters control the time t_m at the maximum of the $\mathrm{RCO2}(t)$ peak in Figs. 1, 3–7. The evolution of the amount of L CO species during oxidation is obtained by

integration of (6) after the substitution of S1(t) by expression (13b)

$$\mathrm{L}(t) = \mathrm{L}(0) \Bigg/ \left(\left(\frac{\mathrm{B}(0)}{\mathrm{NT_B}} \right)^{k_3/k_{\mathrm{O_B}}} \left[1 + \left(\frac{\mathrm{NT_B} - \mathrm{B}(0)}{\mathrm{B}(0)} \right) \times \exp(k_{\mathrm{O_B}} x \mathrm{NT_B} \theta_{\mathrm{O_{wads}}} t) \right]^{k_3/k_{\mathrm{O_B}}} \right), \quad (19)$$

where L(0) is the surface concentration of the L CO species at time 0 of the oxidation. Note that (a) $\mathrm{L}(0) = \mathrm{NT_L}$ because the L CO species does not desorb during the helium purge (high heat of adsorption) and (b) the coverage of the L CO species is $\theta\mathrm{L}(t) = \mathrm{L}(t)/\mathrm{L}(0)$. The substitution of L($t$) (expression (19)) and S1(t) (expression (13b)) in (6) provides RCO2L(t) (unit: molecules of $CO_2/(cm^2\ s)$):

$$\mathrm{RCO2L}(t) = k_3 \mathrm{L}(0) \theta_{\mathrm{O_{wads}}} x \left(\mathrm{NT_B} - \mathrm{B}(0) \right) \times \exp(k_{\mathrm{O_B}} x \mathrm{NT_B} \theta_{\mathrm{O_{wads}}} t) \Bigg/ \left(\left(\frac{\mathrm{B}(0)}{\mathrm{NT_B}} \right)^{k_3/k_{\mathrm{O_B}}+1} \left[1 + \left(\frac{\mathrm{NT_B} - \mathrm{B}(0)}{\mathrm{B}(0)} \right) \times \exp(k_{\mathrm{O_B}} x \mathrm{NT_B} \theta_{\mathrm{O_{wads}}} t) \right]^{k_3/k_{\mathrm{O_B}}+1} \right). \quad (20)$$

The value of the rate at the maximum of the peak, $\mathrm{RCO2L_m}$, is obtained by the introduction of t_m (expression (16)) in (20):

$$\mathrm{RCO2L_m} = k_{\mathrm{O_B}} \mathrm{L}(0) x \mathrm{NT_B} \left(\frac{\mathrm{NT_B}}{\mathrm{B}(0)} \right)^{k_3/k_{\mathrm{O_B}}} \times \left(\frac{k_3}{k_{\mathrm{O_B}} + k_3} \right)^{k_3/k_{\mathrm{O_B}}+1} \sqrt{K_{\mathrm{O_2}} P_{\mathrm{O_2}}}. \quad (21)$$

The kinetic model developed for the oxidation of the L CO species can be applied for the oxidation of the B CO species, provided

$$\mathrm{RCO2B}(t) = -\frac{\mathrm{dB}(t)}{\mathrm{d}t} = k_{\mathrm{O_B}} \mathrm{B}(t) \mathrm{S1}(t) \theta_{\mathrm{O_{wads}}}$$

from the elementary step Sb (S1(t) is given by expressions (13a) or (13b)). The expressions for B(t) and RCO2B(t) are obtained from (19) and (20), respectively, after the replacement of k_3 by k_{OB} and L(t) by B(t). Note that for $D \lesssim 0.5$, the helium purge decreases θ_B to a low value due to the low E_dB values, and S1(0) is very high (S1(t) does not change very significantly during the oxidation). This allows us to use expression (1) for the study of the L-H steps S3 [2–4].

3.4. Exploration of the kinetic model with consideration of the experimental data on the IP

Considering that the contribution of the B CO species to the CO_2 production is negligible at the maximum of the peak, RCO2(t) ≈ RCO2L(t), expressions (18), (17), and (21) allow us to quantify and interpret the impacts of the various experimental parameters on t_m and $\mathrm{RCO2_m}$ in Figs. 1, 3–7.

3.4.1. On the observation of an induction period

Expression (18) indicates that a peak can be detected for RCO2L(t) only if B(0) (the number of B CO species at time $t = 0$ of the oxidation) is higher than a particular value (like (20), expression (18) is a criterion for the observation of a peak). For instance, assuming $k_{\mathrm{O_B}} \approx k_3$, B(0) must be higher than $\mathrm{NT_B}/2$: if the number of B CO species is lower than this value, then RCO2L(t) is similar to a decreasing exponential (a true decreasing exponential profile is obtained for B(0) ≈ 0 [2–4]). Clearly, the presence of an IP is dependent on the B(0) value that is determined by the desorption of the B CO species before oxidation according to (a) the E_dB values (equal to $\mathrm{EB}_{\theta_\mathrm{B}}$, the heat of adsorption) that are dependent on D [10] and (b) the duration t_d of the desorption. For instance, if E_dB is low ($D < 0.5$), then the B CO species significantly desorbs during a short (< 80 s) helium purge and B(0) is very low; the criterion (18) for the observation of an IP cannot be obeyed (the profile of RCO2(t) is similar to a decreasing exponential). This is the situation for the present 2.9% Pt/Al_2O_3 catalyst with $D \lesssim 0.5$ [2,3], because $\mathrm{EB_1} = 45$ and $\mathrm{EB_0} = 94$ kJ/mol [8]. For $D > 0.6$, it has been shown that $\mathrm{EB_1}$ increases significantly and therefore the amount of B CO species decreases more slowly with t_d. This makes it possible to obtain a B(0) value that conforms to the criterion (18), leading to the detection of a peak for RCO2(t). Note that the criterion (18) is also dependent on k_3 and $k_{\mathrm{O_B}}$, which can be affected by experimental factors such as D or the number of O/R cycles. Moreover, if $\mathrm{NT_B}$ decreases (i.e., high Pt dispersions penalize the B CO species [24,25]), then t_m increases (expression (17)), whereas $\mathrm{RCO2L_m}$ decreases (expression (21)). This factor comes into play, in addition to the increase in E_{θ_B} with the increase in D. This is the situation observed for $D > 0.84$: a peak for RCO2(t) is not detected after 10 min of isothermal oxidation at 300 K [10].

3.4.2. Impact of the O_2 partial pressure

Expression (17) shows that when all of the other parameters are unchanged (i.e., $\mathrm{NT_B}$, which is dependent on D and B(0) for the same duration of desorption t_d), t_m is proportional to $1/\sqrt{P_{\mathrm{O_2}}}$, as observed experimentally in Fig. 7; the ratio t_m ($P_{\mathrm{O_2}} = 2$ kPa)/t_m ($P_{\mathrm{O_2}} = 4$ kPa) = 1.48, which is consistent with the expected theoretical value $\sqrt{2}$. Similarly, expression (21) shows that $\mathrm{RCO2L_m}$ is proportional to $\sqrt{P_{\mathrm{O_2}}}$, as observed in Fig. 7; $\mathrm{RCO2L_m}$ ($P_{\mathrm{O_2}} = 4$ kPa)/$\mathrm{RCO2L_m}$ ($P_{\mathrm{O_2}} = 2$ kPa) = 1.398, which is consistent with the theoretical value $\sqrt{2}$. Note that the impact of $P_{\mathrm{O_2}}$ clearly confirms the fact that it is step Sb and not step Sa that controls the formation of the $s1$ sites during oxidation. In other words, step Sa creates the $s1$ sites during the purge in helium before the oxidation, and it is step Sb that increases the number of $s1$ sites during the oxidation.

3.4.3. Impact of the oxidation temperature

Zhou and Gulari have shown without a kinetic model (their theoretical support is that of Bonzel and Ku [15]) that

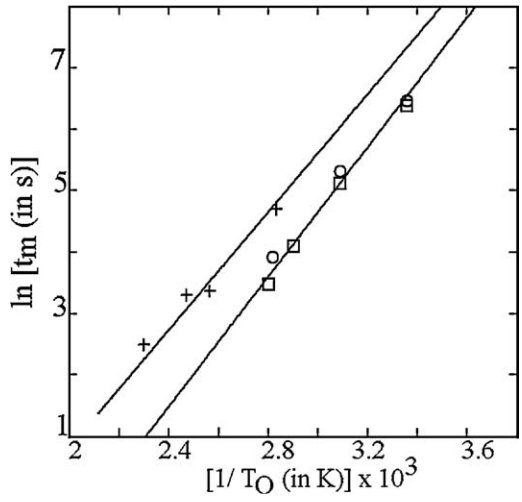

Fig. 8. Evolution of $\ln(t_m)$ as a function on $1/T_O$ on Pt/Al_2O_3 catalysts: (a) □, 1.2% Pt/Al_2O_3 ($D = 0.78$); (b) ○, 2.9% Pt/Al_2O_3 ($D = 0.73$); (c) +, from the data of Li et al. [14].

$\ln(t_m) = f(1/T_O)$ is a straight line with a positive slope for the isothermal oxidation of adsorbed CO on Pd/Al_2O_3. Expression (17) shows that

$$\ln t_m = \frac{E_{O_B} - E_{O_2}/2}{R_{T_O}} + C1. \tag{22}$$

In expression (22), C1 can be considered to be constant because the variation of the logarithmic term in (17) with T_O is limited in particular for similar k_{O_B} and k_3 values. Expression (22) shows that the slope of $\ln(t_m) = f(1/T_O)$ provides $E_{O_B} - (E_{O_2}/2)$. Curves a and b in Fig. 8 show that straight lines are effectively observed for the 1.2 and 2.9% Pt/Al_2O_3 catalysts (for the data in Fig. 5 for 2.9% Pt/Al_2O_3) with similar slopes, providing $E_{O_B} - (E_{O_2}/2) = 44$ kJ/mol. Curve c in Fig. 8 is obtained from the data of Li et al. [14] (see Table 1 in [14]) for a 1% Pt/Al_2O_3 catalyst: the slope provides $E_{O_B} - (E_{O_2}/2) \approx 40$ kJ/mol, a value in very good agreement with the present study, considering the differences in the experimental procedures, showing that $E_{O_B} - (E_{O_2}/2)$ is the same on the three Pt catalysts, whereas for palladium, Zhou and Gulari found a value of 90 kJ/mol [13]. Moreover, the fact that the slopes of $\ln(t_m) = f(1/T_O)$ are positive (Fig. 8) indicates that $E_{O_B} > E_{O_2}/2$. The activation energy of oxidation of adsorbed CO species on various Pt surfaces is in the range of 65–90 kJ/mol [15,21,27–31]. The positive slope in Fig. 8 requires that $E_{O_2} \lesssim 100$ kJ/mol, a value significantly lower that that measured after adsorption of O_2 at 300 K on a Pt surface, that is, 175 kJ/mol at full coverage on the present 2.9% Pt/Al_2O_3 catalyst [5] (this value can be compared with that at low coverage on a Pt(110) surface, 332 kJ/mol [32]). The low E_{O_2} value linked to the positive slopes in Fig. 8 is consistent with the view that the adsorbed oxygen species involved in the CO/O_2 reaction at low temperatures [4,6] is weakly adsorbed (because of the presence of the adsorbed CO species).

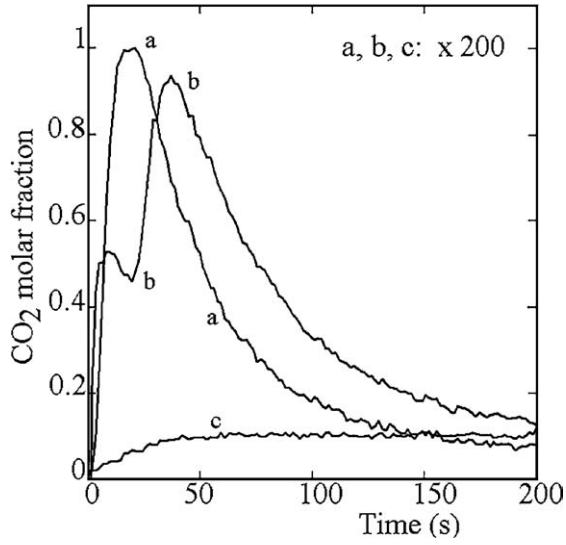

Fig. 9. Molar fractions of CO_2 at the outlet of the micro reactor during the oxidation at 300 K of the adsorbed CO species on 2.9% Pt/Al_2O_3 with $D = 0.48$: (a) $t_d = 2$ min of desorption in helium with 2% O_2/2% Ar/He; (b) without desorption $t_d = 0$ using 2% O_2/2% Ar/He), and (c) without desorption $t_d = 0$ using 0.1% CO/2% O_2/2% Ar/He.

3.4.4. *Impact of the desorption duration t_d*

Expression (17) shows that the sign of $d(t_m)/d(B(0))$ is positive: the increase in B(0) increases t_m. This means that for a given EB_{θ_B} value (this parameter is dependent on D), the shorter the desorption duration is, the higher B(0) is and the longer t_m is, as observed in Fig. 6 and in agreement with the observations of Zhou and Gulari [13]. On 2.9% Pt/Al_2O_3 for $D < 0.5$, we have not detected an induction period [3] because for low EB_{θ_B} values, a short helium purge ($t_d \leqslant 120$ s) decreases B(0) markedly and the criterion (18) is not obeyed. This situation is observed, for instance (Fig. 9a), on 2.9% Pt/Al_2O_3 for $D = 0.48$ with 2% O_2/2% Ar/He after $t_d = 120$ s. Note that in Fig. 9a, the initial increase in RCO2(t) is related in part to the increase in P_{O_2} during the switch (mixing curve). For the same dispersion, Fig. 9b shows that a short induction period is observed for $t_d = 0$ corresponding to the switch 1% CO/1% Ar/He→ 2% O_2/2% Ar/He. This is due to the fact that B(0) is high in the absence of the desorption stage: for $D = 0.48$, $\theta_B \approx 0.85$ at the adsorption equilibrium with $P_{CO} = 1$ kPa [8,10], and the criterion (18) is now obeyed. Moreover, Fig. 9b clearly reveals a first CO_2 peak that is probably due to the oxidation of the B CO species. This interpretation is supported by the amount of CO_2 produced in this first peak after the deconvolution with the main CO_2 peak, ≈4 μmol/g, which is compatible with the amount of B CO species on the Pt surface. For $t_d = 0$, a large fraction of the B CO species is oxidized during the 1% CO/1% Ar/He → 2% O_2/2% Ar/He switch, justifying the approximation that step Sa is negligible compared with step Sb in the presence of oxygen.

3.4.5. *The impact of the number of O/R cycles*

It has been observed that t_m increases with the number of O/R cycles (Figs. 4 and 5). This can be linked to the O_{sads}

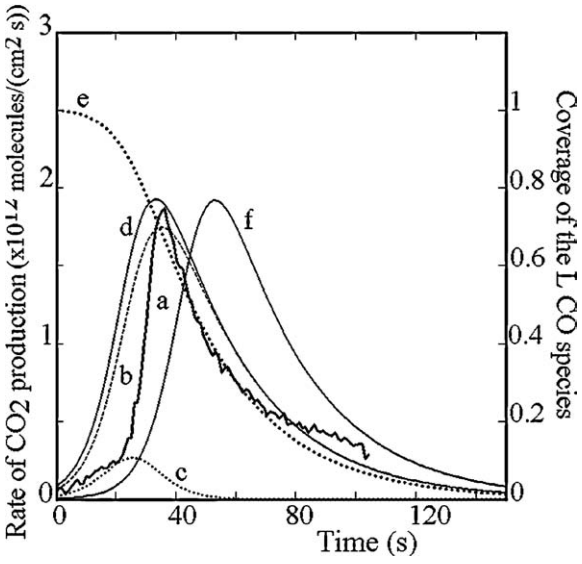

Fig. 10. Simulation of the rate of the CO_2 production and of the coverage of the L CO species during the isothermal oxidation at 324 K on 1.2% Pt/Al_2O_3 ($D = 0.73$) with $P_{O_2} = 2$ kPa (see the text for more details): (a) RCO2(t) from the experimental data; (b) and (c) RCO2L(t) and RCO2B(t) from expression (20); (d) theoretical RCO2(t) (= RCO2L(t) + RCO2B(t)); (e) θL(t) from expression (19), and (f) RCO2(t) with a higher B(0) value.

species formed in the course of the oxidation in parallel with the removal of the adsorbed CO species. It has been shown [5] that a fraction of these O_{sads} species are not reduced to CO_2 during the reduction stage in CO at $T < 323$ K. According to expression (17), the increase in t_m due to the O_{sads} species remaining on the surface can be linked to a decrease in NT_B (i.e., poisoning, reconstruction of the Pt surface) and/or an increase in k_{O_B}.

3.4.6. Simulation of the RCO2L(t), RCO2B(t), RCO2(t), and $\theta_L(t)$

Expressions (19) and (20) and the similar expressions for the B CO species make it possible to compare theoretical and experimental curves for RCO2(t) = RCO2L(t) + RCO2B(t) and $\theta_L(t)$. Fig. 10a gives the experimental curve for RCO2(t) at 324 K during isothermal oxidation with 2% O_2/2% Ar/He on 1.2% Pt/Al_2O_3 with a dispersion $D = 0.65$ after $t_d = 80$ s. For the theoretical curves, K_{O_2} is provided by the statistical thermodynamic for localized adsorbed species [4 and references cited therein]. Because of the large number of kinetic parameters affecting the theoretical curves, the values used in the simulation must be considered semi-quantitative. Curves b, c, d, and e in Fig. 10 give RCO2L(t), RCO2B(t), RCO2(t) = RCO2L(t) + RCO2B(t), and L(t), respectively, for the following values: (a) $T = 324$ K, $P_{O_2} = 2$ kPa, $L(0) = NT_L = 0.9 \times 10^{14}$ molecules/cm^2, and $NT_B = 0.7 \times 10^{13}$ sites/cm^2 because of the experimental condition; (b) $E_3 = 70$ kJ/mol and $E_{O_B} = 66$ kJ/mol ([15, 21,27–31] and previous studies [2,3]); (c) $E_{O_2} = 36$ kJ/mol (estimated values [2,3]) and $B(0) = 0.98\ NT_B$ and $x = 1/4$ (arbitrary, to obtain theoretical curves similar to the experimental curves). Several other sets of values provide theoretical curves similar to curves b–e due to the opposite impacts of some parameters. However, the activation energies of oxidation and the heat of adsorption of O_2 cannot be sharply different (factor $\lesssim 1.2$) from those used in Figs. 10b–e. In particular, the simulation indicates that the values of E_3 and E_{O_B} must be similar (with a difference of a few kJ/mol). Note that $E_{O_B} - E_{O_2}/2 = 48$ kJ/mol is consistent with the value determined from Fig. 8. In Fig. 6, it is observed that the decrease in t_d increases t_m without a strong modification of $RCO2_m$. This situation can be simulated by an increase in B(0) to $0.999\ NT_B$ (i.e., for $t_d = 0$) without changing the other parameters, as shown in Fig. 10f; the $RCO2_m$ values are similar in curves d and f, whereas the t_m values are different. The simulations in Fig. 10 show the difficulties that are encountered for a numerical solution for the set of differential equations from steps Sa, S2, Sb, and S3 based on the best agreement between theoretical and experimental curves; the large number of kinetic parameters and their possible dependence on the coverage of the Pt surface may lead to various sets of kinetic parameters. The merit of the mathematical expressions (17)–(21) is that they show how the different parameters affect simple experimental data such as t_m and $RCO2_m$.

3.5. Contribution of the kinetic model to the microkinetic approach to the CO/O_2 reaction

The kinetic model of the oxidation of the adsorbed CO species on Pt/Al_2O_3 supports the view that the Pt^0 sites allowing the formation of the O_{wads} species are those adsorbing the B CO species (and/or the 3FC CO species). One of the key points of this interpretation is that the high EL_{θ_L} values (i.e., $EL_1 = 110$ kJ/mol) do not allow the desorption of the L CO species at $T < 380$ K, in contrast to the B CO species that have low EB_{θ_B} values ($EB_1 = 45$ kJ/mol and $EB_1 = 57$ kJ/mol for $D \lesssim 0.6$ and $D \gtrsim 0.6$, respectively). It is well known that a increase in P_{CO} decreases the rate of the CO/O_2 reaction at low temperatures, and -1 kinetic order is observed for the CO reactant [11,21,22,33]. This impact of P_{CO} can be explained by the fact that the EB_1 values make it possible to maintain $\theta_B > 0.85$ at 300 K for $P_{CO} = 1$ kPa, regardless of the value of D (with $\theta_B \approx 1$ for $D > 0.85$) [10]. In the presence of CO, these high θ_B values limit the number of $s1$ sites available for the adsorption of the O_{wads} species (note that the low heat of adsorption of O_{wads} prevents a desorption of the B CO by a competitive chemisorption). This impact of P_{CO} is well revealed by a study of the evolution of RCO2(t) during the isothermal oxidation of the adsorbed CO species in the presence of a small amount of CO_g. For instance, Fig. 9c gives RCO2(t) at 300 K on 2.9% Pt/Al_2O_3 for $D = 0.48$ with the switch 1% CO/1% Ar/He → 0.1% CO/2% O_2/2% Ar/He. The comparison with Fig. 9b (switch: 1% CO/1% Ar/He → 2% O_2/2% Ar/He) clearly shows that the small CO partial pressure suppresses the CO_2 peak. Note that RCO2(t) increases progressively (Fig. 9c) to a roughly constant value (rate of the CO/O_2 reaction); this probably

corresponds to a change in the adsorption equilibrium coverage θ_B associated with the decrease in P_{CO} from 1 kPa to 0.1 kPa. Only an increase in T_O may decrease θ_B significantly (θ_B decreases because of (a) the modification of adsorption equilibrium and (b) the oxidation reaction according to step Sb). A decrease in θ_B increases QO_{wads}, favoring the oxidation of the L CO species and the TOF of the CO/O_2. This leads to the conclusion that the lower TOF values at high Pt dispersions [10,11] come from the increase in EB_{θ_B} with D: the higher EB_{θ_B} is, the lower the number of $s1$ sites is (adsorbing the O_{wads} species) and the lower the TOF is. It must be noted that the impact of P_{CO} on $RCO_2(t)$ (Fig. 9c) underscores the importance of the design of the experiments linked to the study of IP; for a large dead volume of the reactor, the decrease in P_{CO} according to the mixing curve can be very progressive, leading to long induction periods. This probably explains the observations of Dwyer and Bennett [12] on the impact of the gas flow rate on the IP, studied with an IR cell reactor.

3.6. Comparison of the present kinetic model for Pt/Al_2O_3 with that for a Pt single crystal [15]

Bonzel and Ku [15] have performed experiments on Pt(110) similar to the present study according to the following procedure. A flow of a CO/O_2 mixture at a low pressure is introduced onto Pt(110) surface at a temperature in the range of 393–453 K, and the rate of CO_2 production is followed with a mass spectrometer. Then the partial pressure of CO is suddenly decreased to perform an isothermal oxidation of the adsorbed CO species. The rate of the CO_2 production, $RCO2(t)$, is followed as a function of time on stream in O_2. As in the present study, the authors observe an induction period; $RCO2(t)$ is very low at $t = 0$ (steady state of the CO/O_2 reaction) and increases progressively, followed by a strong increase, leading to the detection of a well-defined asymmetrical $RCO2(t)$ peak with a maximum characterized by t_m and $RCO2_m$. Moreover, t_m decreases with increasing T_O from ≈ 240 s to ≈ 30 s at 393 and 453 K, respectively, according to a roughly linear profile for $\ln t_m = f(1/T_O)$ (see Figs. 2–3 in [15]). In contrast to the present study, P_{O_2} has no impact on t_m [15]. To explain their experimental observations, Bonzel and Ku consider the following elementary steps [15]:

BK0 $CO_{ads} + O_2 \rightarrow CO_2 + O_{ads}$ rate constant, k_0;
BK1 $O_2 + 2\sigma \rightarrow 2O_{ads}$ rate constant, k_1;
BK2 $CO_{ads} \rightarrow CO + \sigma$ rate constant, k_2;
BK3 $CO_{ads} + O_{ads} \rightarrow CO_2 + 2\sigma$ rate constant, k_3,

where σ is a Pt site adsorbing either CO_{ads} or O_{ads} (competitive chemisorption). The nature of CO_{ads} (i.e., L, B, or 3FC CO species) is not considered [15]. During the isothermal oxidation of the adsorbed CO species on Pt(110), (a) step BK0 (Eley–Rideal elementary step) is neglected because P_{O_2} has no impact on $RCO2(t)$ and (b) step BK1 is not considered a determining factor because of the large O_2 excess [15] (this is similar to our assumption that O_{wads} is at the adsorption equilibrium). Finally, these various assumptions lead to the situation that the Pt sites available for the oxygen adsorption are due to the desorption and the oxidation of CO_{ads}. The authors apply the mean-field formalism, considering a competitive chemisorption on the same Pt sites that leads to [15]

$$\theta_v + \theta_{O_{ads}} + \theta_{CO_{ads}} = 1. \tag{23}$$

Assuming that the surface is mainly covered by O_{ads} and CO_{ads} ($\theta_v \approx 0$) [15], then (23) provides

$$\theta_{O_{ads}} + \theta_{CO_{ads}} \approx 1. \tag{24}$$

This situation corresponds to two strongly adsorbed CO and oxygen species, and it is similar to the situation studied previously on the present Pt/Al_2O_3 catalyst for the reduction by CO of the O_{sads} species formed by adsorption of O_2 on the freshly reduced catalyst [5].

Steps BK2 and BK3 lead to

$$\frac{-d\theta_{CO_{ads}}}{dt} = k_2\theta_{CO_{ads}} + k_3\theta_{CO_{ads}}\theta_{O_{ads}}, \tag{25}$$

$$RCO2(t) = k_3\theta_{O_{ads}}\theta_{CO_{ads}}. \tag{26}$$

The integration of (25) with the consideration of (24) provides $\theta_{CO_{ads}} = f(t)$ and then $RCO2(t)$ with a maximum at [15]:

$$t_m = \frac{1}{k_2 + k_3} \ln\left[\frac{(2k_2 + k_3)\theta_{CO_{ads}}(0)}{(k_2 + k_3) - k_3\theta_{CO_{ads}}(0)}\right], \tag{27}$$

where $\theta_{CO_{ads}}(0)$ is the coverage of CO_{ads} at time 0 of the isothermal oxidation. Expression (27) differs from expression (17) but also presents some similarities. In particular, the detection of a $RCO2(t)$ peak requires that the logarithm term of (27) is positive, leading to the definition of a criterion similar to (18) for the observation of an IP: this criterion is $\theta_{CO_{ads}}(0) \geqslant 1/2$. The point of interest is that the authors compare the experimental and theoretical curves $RCO2(t)$ (expression (26)), which are similar to the present Fig. 10. They indicate that a reasonable agreement imposes (a) $k_3 \gg k_2$, meaning that the desorption is negligible (high activation energy of desorption of the CO_{ads} species) during the isothermal oxidation (this is also the situation for Pt/Al_2O_3) and (b) $\theta_{CO_{ads}}(0) \approx 1$, in line with the criterion $\theta_{CO_{ads}}(0) \geqslant 1/2$. Expression (27)), associated with $k_3 \gg k_2$, explains that $\ln t_m = f(1/T_O)$ is a straight line (the logarithm of the second term on the right side of (27)) does not vary strongly with $1/T$); the slope provides the activation energy of step BK3, $E_3 \approx 51$ kJ/mol [15]. Finally, the main difference in the experimental data linked to the isothermal oxidation of the adsorbed CO species in [15] and in the present study is that t_m is not dependent on P_{O_2} on Pt(110), in contrast to Pt/Al_2O_3 (Fig. 7). The two kinetic models show that this difference is due to the fact that the elementary steps involved in the oxidation of the adsorbed CO species are different: a reaction between

strongly adsorbed CO and oxygen species on the same sites on Pt(110) and a reaction between a strongly adsorbed CO species and a weakly adsorbed oxygen species formed on different sites on Pt/Al_2O_3. This key difference is probably linked to the experimental conditions (material and pressure gaps), as discussed in a previous study [5]. For instance, the low pressures used on Pt(110) prevent the impact of a weakly adsorbed oxygen species during isothermal oxidation. It must be noted that we have shown previously that the two L-H steps can be studied on Pt/Al_2O_3: that between strongly adsorbed CO and oxygen species is implicated during the reduction by CO of O_{sads} species formed by the adsorption of O_2 on a freshly reduced solid [5] (situation denoted Pt–O surface, L-H elementary denoted S3a, [6,10]), whereas that between the strongly adsorbed L CO species and the O_{wads} species corresponds to the oxidation by O_2 of preadsorbed CO species (situation denoted Pt–CO, elementary step denoted S3; [6,10] and present study). The fact that the oxidation temperatures $T_O > 393$ K used by Bonzel and Ku [15] are significantly higher than those in the present study ($T_O < 353$ K) is due to the necessity to decrease the coverage of the L CO species by desorption to create the first sites for the formation of O_{sads}. Simple calculations with the assumption that $EL_1 = 115$ and $EL_0 = 206$ kJ/mol [8] show that $\theta_L = 0.97$ for $t_d = 10$ min at $T = 353$ K. Moreover, a high T_O value is also imposed by the rate constant of the L-H step S3a between strongly adsorbed species. It decreases strongly with the decrease in the coverage of the oxygen species on Pt/Al_2O_3 [5]: the activation energy increases from 65 to 110 kJ/mol at $\theta_{O_{sads}} = 1$ and 0.39, respectively [5] (at $\theta_{O_{sads}} = 1$ the reaction is observed at 223 K [5]). A similar dependence of the rate constant of oxidation with the coverage of the O_{sads} species is observed on single crystals [34,35]. This makes it possible to assume that a significant CO_2 production is observed on Pt(110) for $T_O > 393$ K because $\theta_{O_{sads}}$ increases from a very low value (at $t = 0$ the Pt(110) surface is mainly covered by CO_{ads}). The dependence of the rate constant of oxidation on $\theta_{O_{sads}}$ is consistent with the fact that Bonzel and Ku [15] observe an asymmetrical $RCO2(t)$ peak; it increases slowly and it decreases rapidly. Their kinetic model, assuming a rate constant of oxidation independent on $\theta_{O_{sads}}$, leads to a symmetrical $RCO2(t)$ peak [15]. The asymmetrical peak is due to the increase in the rate constant k_3 with the increase in $\theta_{O_{sads}}$. It can be noted that $E_3 = 51$ kJ/mol, determined by the slope of $\ln(t_m) = f(1/T_O)$ (when the coverage of the O_{sads} species is high), is in reasonable agreement with that obtained on 2.9% Pt/Al_2O_3 for the reaction between O_{sads} and L CO species: 65 kJ/mol at $\theta_{O_{sads}} \approx 1$ [5].

In conclusion, this comparison reinforces the view developed in previous studies [2–6] that the apparent contradictions between single crystals and metal-supported catalysts concerning the CO/O_2 reaction on Pt is mainly linked to the fact that two L-H steps can be considered. The first L-H step (denoted S3a in [5,6]) corresponds to the reaction of strongly adsorbed CO (L CO species) and oxygen species (O_{sads}). It is observed on single crystals and only after the formation of a Pt–O surface on Pt/Al_2O_3 [4,5]. The second L-H step (denoted S3) corresponds to the reaction of a strongly adsorbed CO species (L CO) and a weakly adsorbed oxygen species O_{wads}. It is observed on Pt/Al_2O_3 during the oxidation of the strongly adsorbed L CO species forming a Pt–CO surface [6]. On single crystals, UHV conditions do not allow the involvement of a weakly adsorbed species during the oxidation. Moreover, considering the assignment of the $s1$ sites adsorbing the O_{wads} species to the removal of the B CO species, one may believe that the material gap may lead to a situation where these sites are absent from particular single crystals. For instance, B CO species are not detected on stepped surfaces [26]. Note that whatever the kinetic model (present study or [15]), $\ln(t_m) = f(1/T_O)$ is a straight line. However, the slope provides either the activation energy of the L-H steps (Bonzel and Ku model) or $E_{O_B} - E_{O_2}/2$ (present study).

4. Conclusion

The present study has shown that the isothermal oxidation of the adsorbed CO species on Pt/Al_2O_3 leads to a rate of the CO_2 production, $RCO2(t)$, with the duration t of oxidation characterized by an induction period for high Pt dispersions. A peak is observed that is characterized by t_m and $RCO2_m$ that offers a way to characterize the L-H steps between adsorbed CO species (L and B CO species) and adsorbed oxygen species. Several experimental parameters affect the t_m value, such as the Pt dispersion (D), the oxidation temperature (T_O), the duration (t_d) of the desorption before oxidation, and the oxygen partial pressure (P_{O_2}). A kinetic model involving the adsorption of a weakly adsorbed oxygen species, O_{wads}, on the Pt^0 sites liberated by the removal of the B CO species provides a set of mathematical expressions that provide a reasonable explanation of the impact of the various experimental and kinetic parameters on t_m and $RCO2_m$. A comparison of the present study with the observations and the kinetic model for the isothermal oxidation of the adsorbed CO species on Pt(110) [15] shows that the pressure and material gaps may lead to a situation where the L-H elementary steps studied are not the same: L CO + O_{wads} on Pt/Al_2O_3 and L CO + O_{sads} (O_{sads} is a strongly adsorbed oxygen species) on Pt single crystals. The present study focuses on the impact of a small number of Pt^0 sites linked to the adsorption of the B CO species (and/or the 3FC CO species) on the CO/O_2 reaction. This underscores one of the difficulties of the microkinetic approach to the CO/O_2 reaction: these sites must be differentiated from the total number of Pt^0 sites.

In addition to the academic interest in the microkinetic interpretation of the CO/O_2 reaction as developed in the present study, there is a more application-based perspective: it can be envisaged to orient the preparation of the Pt catalyst to modify a kinetic parameter of interest to favor the TOF,

as imagined by M. Boudart in the foreword of [1]. For instance, for three-way exhaust gas catalysis the objective is to decrease the light-off temperature (temperature at x% of CO conversion, i.e., $x = 50$). The microkinetic approach developed in [2–10] shows that two orientations can be envisaged to increase the TOF. The first orientation consists of favoring the mechanism denoted M2 in [6] involving strongly adsorbed L CO and oxygen species. This mechanism allows the oxidation of the L CO species even at $T < 273$ K but is not sustained during the CO/O_2 reaction [6]. The second orientation consists of improving the performance of the mechanism denoted M1 involving the strongly adsorbed L CO species and the weakly adsorbed oxygen species, for instance, by modification of the Pt sites adsorbing the B CO species either through an increase of their number and/or a decrease of the heat of adsorption of the B CO species (i.e., by a decrease in D [4,6] or by modification of the Pt particles by a second metal).

Acknowledgments

We acknowledge with pleasure FAURECIA Systèmes d'échappements, Bois sur prés, 25 550, Bavans, France, for its financial support and the MENRT (Ministère de l'Education Nationale, de la Recherche et de la Technologie) for the research fellowship of S.D.

Nomenclature and additional data

Main parameters

T_O Oxidation temperature (denoted T if there is no ambiguity);
P_{CO} and P_{O_2} CO and O_2 partial pressures;
t_a, t_d, and t_O Durations of the isothermal adsorption, desorption, and oxidation of the adsorbed CO species, respectively;
t and t' The time on stream in O_2 and in helium during the oxidation and desorption stages.

Pt^0 sites and adsorbed species

L, B, and 3FC Linear, bridged, and threefold coordinated CO species, respectively;
O_{wads} Weakly adsorbed oxygen species formed in the presence of adsorbed CO species;
O_{sads} Strongly adsorbed oxygen species;
Pt^0_B, Pt^0_L, and $s1$ Pt^0 sites adsorbing the B, L, and O_{wads} species, respectively ($s1$ sites are formed by the removal of the B CO species);
θ_L, θ_B, and $\theta_{O_{wads}}$ Coverages of the adsorbed L CO, B CO, and O_{wads} species.

Rate of CO_2 production during the isothermal oxidation by O_2 of the adsorbed CO species

RCO2L(t)) and RCO2B(t)) Theoretical rates of oxidation of the L and B CO species, respectively (t time on stream in O_2);
RCO2(t)) Experimental and theoretical rates for the CO_2 production with RCO2(t) = RCO2L(t) + RCO2B(t);
$RCO2_m$ and t_m Characteristics of the peak maximum of RCO2(t).

Amount of adsorbed species per unit surface area of Pt (i.e., $\mu mol/cm^2$ of Pt surface)

QO_{wads} Amount of O_{wads};
NT_L and NT_B Highest numbers of L and B CO species on the Pt surface ($NT_B \lesssim 0.1\ NT_L$);
L(t) and B(t) Amounts of L and B CO species after a duration t of the oxidation ($L(0) = NT_L$);
S1(t) Amount of $s1$ sites after a duration t of oxidation.

Kinetic parameters

k_3 (E_3), k_{O_B} (E_{O_B}) Rate constants (activation energies) of the L-H steps for the oxidation of the L and B CO species, respectively;
k_{dB}, E_{dB} Rate constant and activation energy of desorption of the B CO species;
K_{O_2}, E_{O_2}, k_{aO_2}, and k_{dO_2} Adsorption coefficient, heat of adsorption, adsorption, and desorption rate constants of the O_{wads} species respectively;
EL_{θ_L}, EB_{θ_B} Heats of adsorption of the L and B CO species at several coverages (equal to the activation energies of desorption: nonactivated CO chemisorption);
M1 and M2 Kinetic models of the CO/O_2 reaction (see [6] for more details).

Additional data

Detailed development of expressions (8)–(21) is available via an e-mail to D.B.

References

[1] J.A. Dumesic, D.F. Rudd, L.M. Aparicio, J.E. Rekoske, A.A. Trevino, The Microkinetics of Heterogeneous Catalysis, 1993, ACS Prof. Ref. Book.
[2] A. Bourane, D. Bianchi, J. Catal. 202 (2001) 34.
[3] A. Bourane, D. Bianchi, J. Catal. 209 (2002) 114.
[4] A. Bourane, D. Bianchi, J. Catal. 209 (2002) 126.
[5] A. Bourane, D. Bianchi, J. Catal. 220 (2003) 3.
[6] A. Bourane, D. Bianchi, J. Catal. 222 (2004) 499.
[7] O. Dulaurent, D. Bianchi, Appl. Catal. 196 (2000) 271.
[8] A. Bourane, O. Dulaurent, D. Bianchi, J. Catal. 196 (2000) 115.
[9] A. Bourane, D. Bianchi, J. Catal. 218 (2003) 447.

[10] A. Bourane, S. Derrouiche, D. Bianchi, J. Catal., in press.
[11] G.S. Zafiris, R.J. Gorte, J. Catal. 140 (1993) 418.
[12] S.M. Dwyer, C.O. Bennett, J. Catal. 75 (1982) 275.
[13] X. Zhou, E. Gulari, Langmuir 2 (1986) 709.
[14] Y. Li, D. Boecker, R.D. Gonzalez, J. Catal. 110 (1988) 319.
[15] H.P. Bonzel, R. Ku, Surf. Sci. 33 (1972) 91.
[16] R.A. Demmin, R.J. Gorte, J. Catal. 90 (1984) 32.
[17] S. Derrouiche, D. Bianchi, Langmuir 20 (2004) 4489.
[18] J.S. Rieck, A.T. Bell, J. Catal. 85 (1984) 621.
[19] C.N. Satterfield, T.K. Sherwood, The Role of Diffusion in Catalysis, Addison–Wesley, 1963.
[20] H. Ahlafi, C.O. Bennett, D. Bianchi, J. Catal. 133 (1992) 83.
[21] R.K. Herz, S.P. Marin, J. Catal. 65 (1980) 281.
[22] S.H. Oh, G.B. Fisher, J.E. Carpenter, D.W. Goodmann, J. Catal. 100 (1986) 370.
[23] M. Rinnemo, D. Kulginov, S. Johansson, K.L. Wong, V.P. Zhadanov, B. Kasemo, Surf. Sci. 376 (1997) 297.
[24] J. Sarkany, R.D. Gonzalez, Appl. Catal. 4 (1982) 53.
[25] M.A. Vannice, L.C. Hasselbring, B. Sen, J. Catal. 97 (1986) 66.
[26] B.E. Hayden, K. Kretzschmar, A.M. Bradshaw, R.G. Greenler, Surf. Sci. 149 (1985) 394.
[27] C.T. Campbell, G. Ertl, H. Kuipers, J. Segner, J. Chem. Phys. 73 (1980) 5862.
[28] T. Engel, G. Ertl, Adv. Catal. 28 (1979) 1.
[29] N.W. Cant, R.A. Donaldson, J. Catal. 71 (1981) 320.
[30] G.W. Coulston, G.L. Haller, ACS Symp. Ser. 482 (1992) 59.
[31] R.H. Nibbelke, A.J.L. Nievergeld, J.H.B.J. Hoebink, G.B. Marin, Appl. Catal. B 19 (1998) 245.
[32] C.E. Wartnaby, A. Stuck, Y.Y. Yeo, D.A. King, J. Phys. Chem. 100 (1996) 12483.
[33] R.H. Nibbelke, M.A.J. Campman, J.H.B.J. Hoebink, G.B. Marin, J. Catal. 171 (1997) 358.
[34] C.T. Campbell, G. Ertl, H. Kuipers, J. Segner, J. Chem. Phys. 73 (1980) 5862.
[35] F. Zaera, J. Liu, M. Xu, J. Chem. Phys. 106 (1997) 4204.